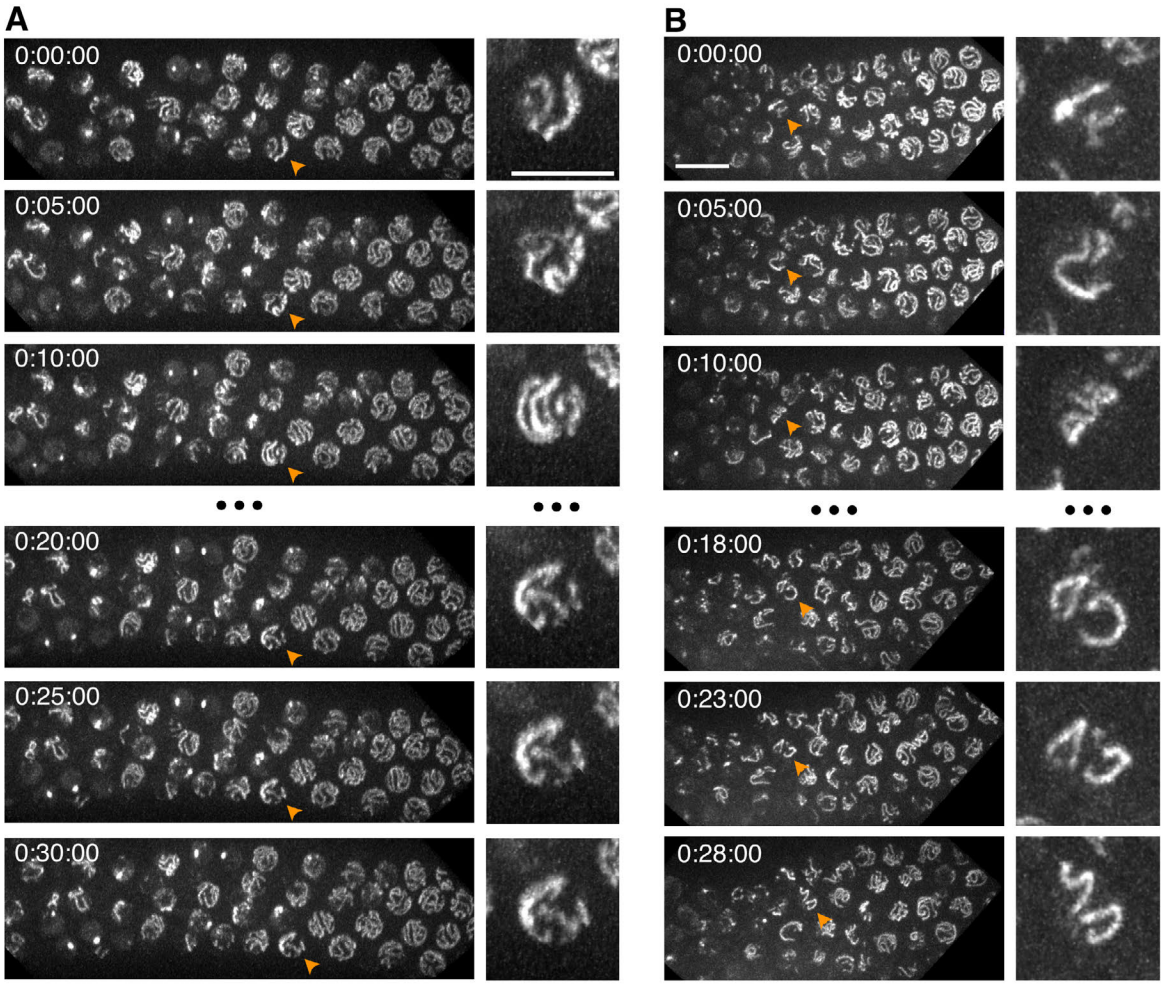

C

	Pharyngeal activity	No pharyngeal activity	Total
Chromosome movement	**23**	**3**	26
No chromosome movement	**17**	**21**	38
Total	40	24	64

D

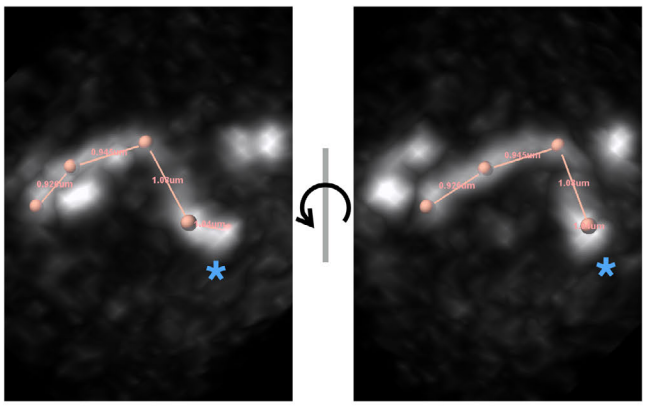

Rog and Dernburg, Figure S1

Figure S1, related to Figure 1: Effects of exogenous serotonin during long-term imaging, and an example of 3D SC filament tracing

(A-B) Maximum intensity projections of selected 3D images from time-lapse imaging of *EmGFP-SYP-3; syp-3* hermaphrodites. Meiosis progresses from left to right. 3D images were taken at 1-minute intervals. The nuclei highlighted on the right are marked by orange arrowheads. Nuclei and filaments are easily tracked despite the movement of internal organs and the dynein-driven chromosome motions that occur throughout this stage of meiosis. (A) Active meiotic chromosome motion ceases after approximately 15 minutes (around 0:03 sec in Movie 1). Scale bars = 5μm. (B) Active chromosome motion persists for more than 1 hour in the presence of 25mM serotonin (see Movie 2). Scale bar = 10 μm.

(C) Persistence of meiotic chromosome movement is correlated with pharyngeal pumping. *EmGFP-SYP-3; syp-3* hermaphrodites were immobilized for 1 hour before meiotic chromosome motion and pharyngeal activity were assayed. Fisher's exact test: $p<10^{-6}$.

(D) Example of filament tracing, based on the image in Figure 4B, timepoint 0:09:00. (right) Projection of the original image stack overlaid with 5 points (one at each end of the filament and 3 in the middle). The points are connected with straight lines, and the length of each line is noted next to it. The sum of the lengths of the 4 intervals is 4.0μm. Note that at its right end the filament turns into the image, and therefore the last point is not visible in this projection (blue asterisk). (left) The image on the right was tilted to the left to expose the 3-dimensional nature of the tracing, and the fifth end point that was not visible.

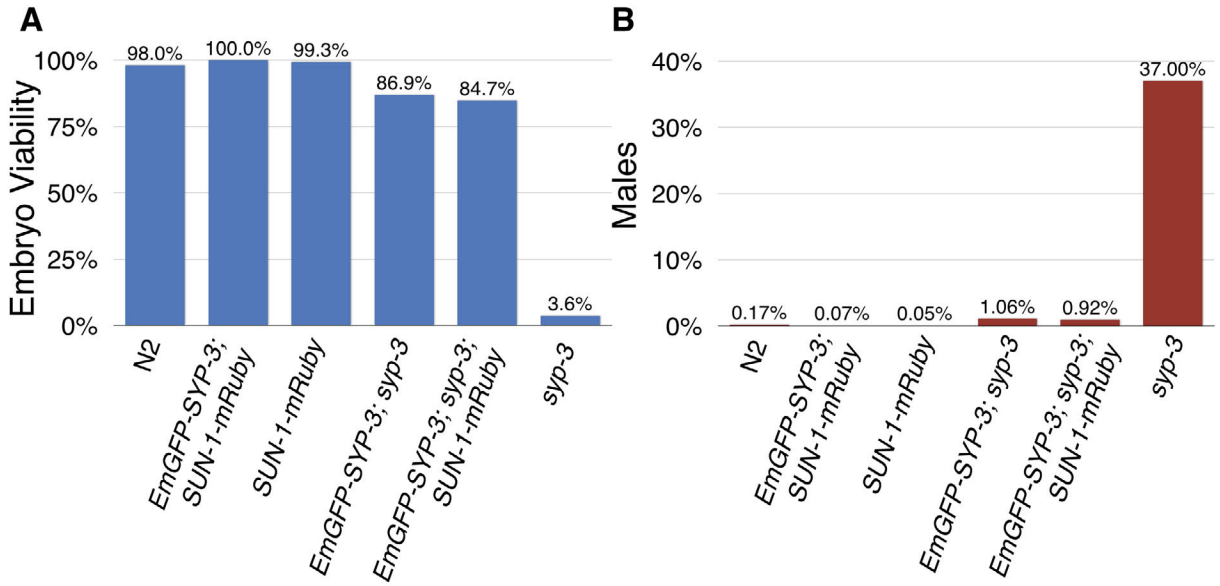

C

genotype	viability	males	brood size	n
wild type (N2 Bristol)	0.98	0.0017	294	1228, 1468,6
EmGFP-SYP-3; SUN-1-mRuby	1	0.0007	278	972, 1392, 5
SUN-1-mRuby	0.993	0.0005	315	1102, 1884, 6
EmGFP-SYP-3; syp-3	0.869	0.0106	183	1105, 1136, 7
EmGFP-SYP-3; syp-3; SUN-1-mRuby	0.847	0.0092	199	815, 872, 5

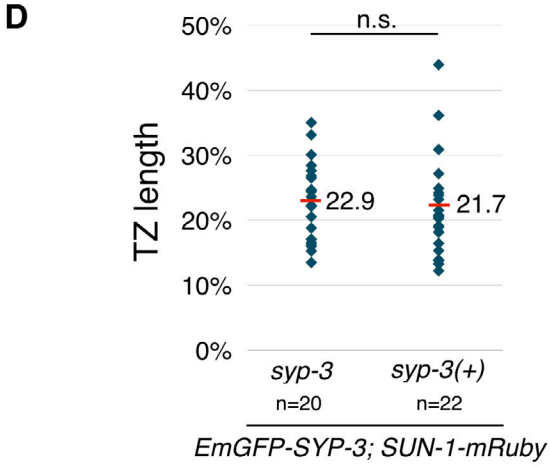

Rog and Dernburg, Figure S2

Figure S2, related to Figure 1: Phenotypic analysis of strains expressing SC reporters
(A-B) The fraction of viable embryos (A) and males (B) among the progeny of self-fertilizing hermaphrodites of the indicated genotypes. Data for *syp-3(ok758)* are from (Smolikov et al., 2007).
(C) Embryo viability, male self-progeny, and brood sizes from hermaphrodites of the indicated genotypes. n values indicate the total number of fertilized eggs, adult progeny, and broods analyzed, respectively.
(D) Transition zone length expressed as fraction of the total gonad length for worms expressing EmGFP-SYP-3 and SUN-1-mRuby, and either carrying the *syp-3(ok758)* mutation or the wild-type *syp-3* gene [*syp-3(+)*]. No significant difference between the two genotypes was observed (two-sided Student's t-test; n.s., not significant).

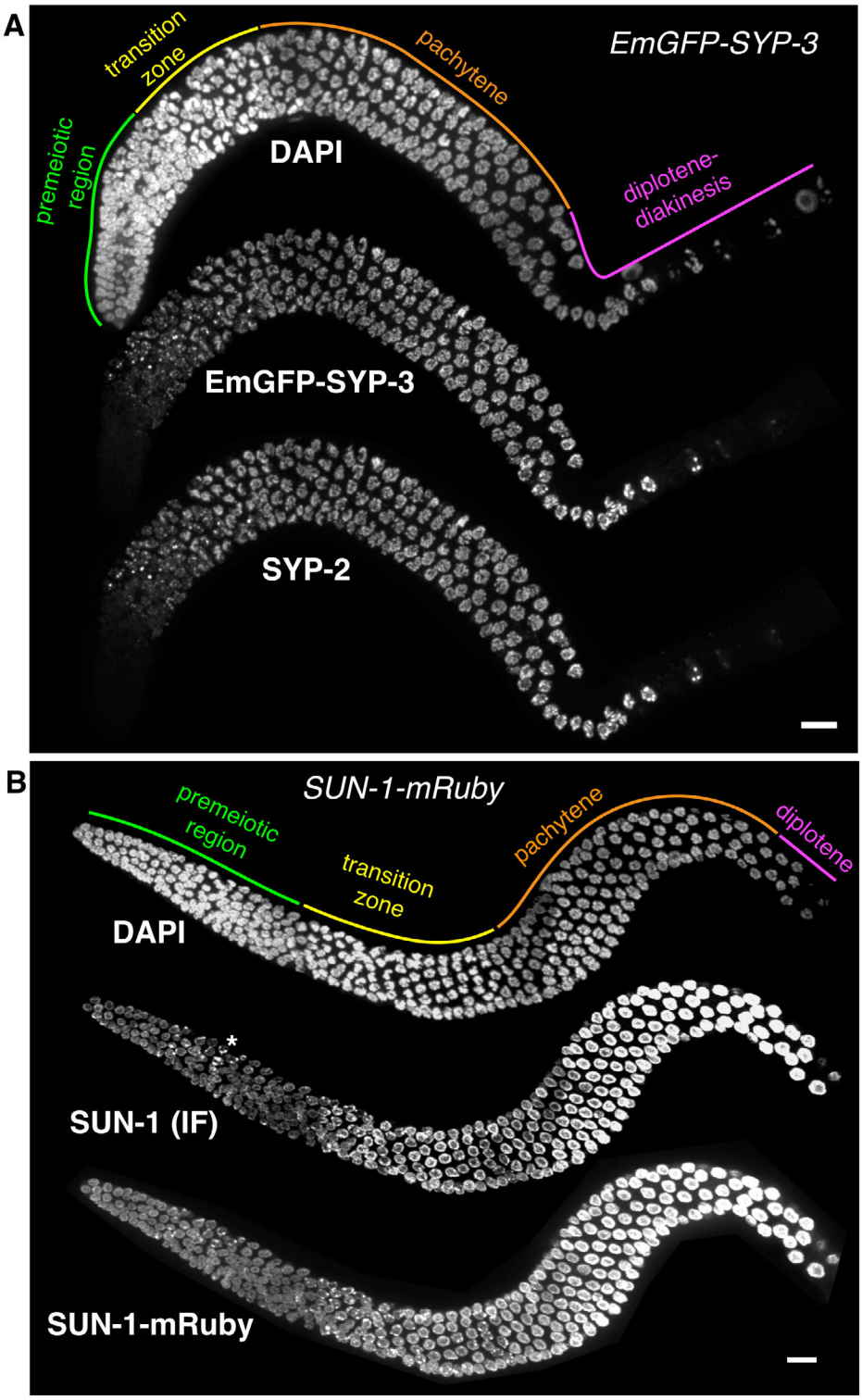

Rog and Dernburg, Figure S3

Figure S3, related to Figure 1: Localization of fluorescent reporters throughout the gonad
(A) A representative gonad from an *EmGFP-SYP-3* adult hermaphrodite stained for DNA (DAPI) and SYP-2. EmGFP-SYP-3 was visualized by its intrinsic fluorescence. The different stages of meiosis were identified by chromatin morphology. EmGFP-SYP-3 and SYP-2 immunofluorescence show indistinguishable distributions. Scale bar = 10 μm.
(B) A representative gonad from a *SUN-1-mRuby* adult hermaphrodite stained with DAPI and SUN-1 antibodies. SUN-1-mRuby was visualized by its intrinsic fluorescence. Meiotic staging was based on chromatin morphology. Distinct patches of SUN-1 are observed in the transition zone, and also enriched near centrosomes in mitotic nuclei (marked with an asterisk). Scale bar = 10 μm.

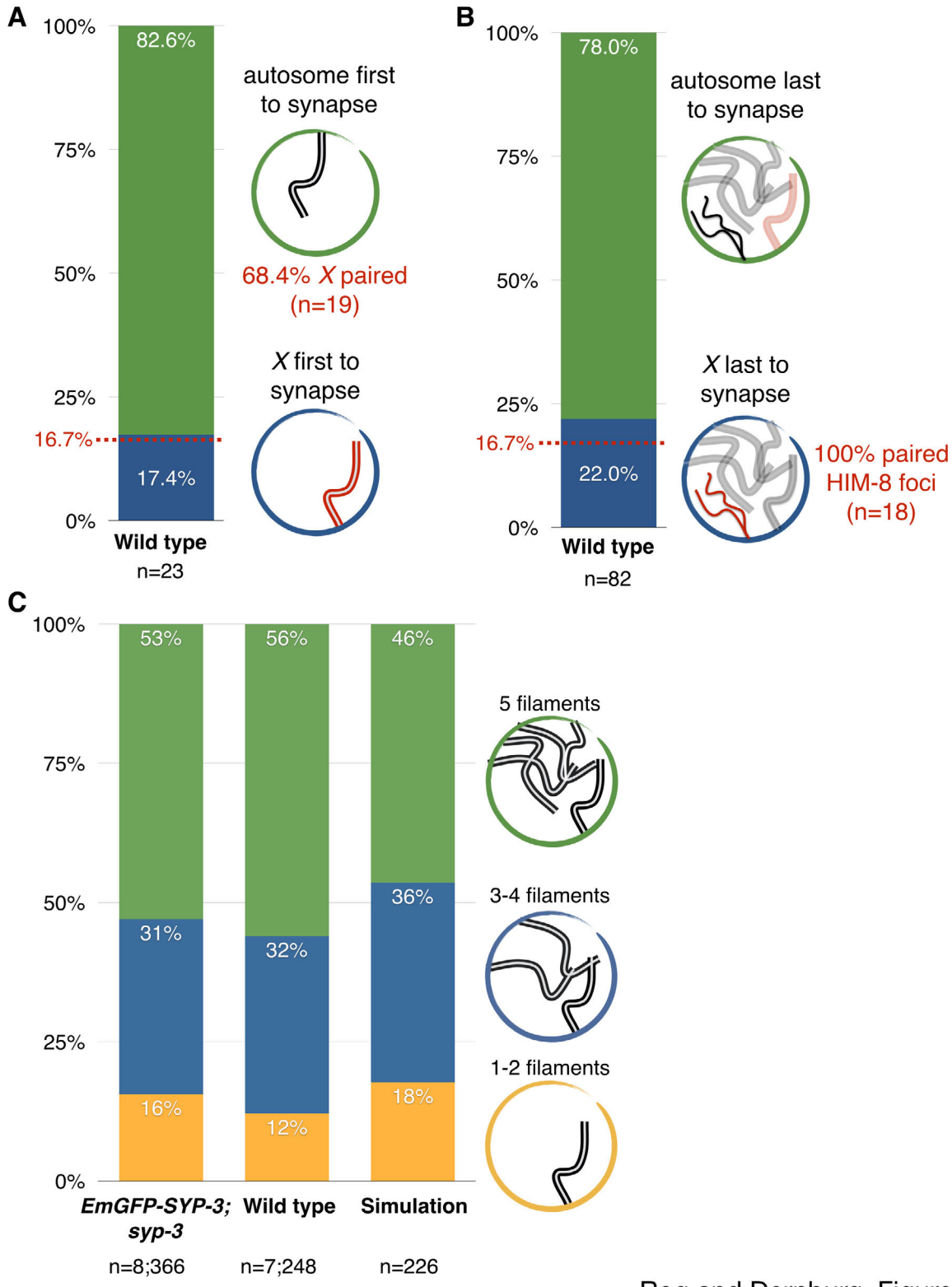

Rog and Dernburg, Figure S4

Figure S4, related to Figure 3: Dynamics of SC initiation across the nucleus

(A-B) We tested whether the order by which chromosomes synapse is random or stereotyped. Synapsed and unsynapsed chromosomes were identified using antibodies against the axis component HTP-3 and the SC component SYP-2. Synapsed regions are positive for both SYP-2 and HTP-3, while unsynapsed regions show only HTP-3 staining. *X* chromosome PCs were marked by antibodies against HIM-8. The pairing status of the *X* chromosomes was also scored based on the proximity of HIM-8 foci. Nuclei in which only a single chromosome pair has synapsed (A), or only a single pair remains unsynapsed (B), can be recognized by inspection. If the order is random, the *X* chromosomes should synapse first in 1/6 of nuclei and last in the same fraction (16.7%; red dashed line). Our data were consistent with this hypothesis. In addition, we observed that in 68.4% of nuclei with only a single synapsed autosome, HIM-8 foci were already paired. In nuclei where only the *X* chromosomes remained unsynapsed, HIM-8 foci were always paired. This, together with other evidence, indicates that pairing of homologous PCs is unlikely to be rate-limiting for initiation of synapsis.

(C) To test whether the rate of synapsis initiation is affected by the synapsis status of other chromosomes, we analyzed the distribution of full-length SCs in images of fixed nuclei stained for HTP-3 and SYP-2, as above. Nuclei were classified as 'early' (1-2 filaments), 'late' (5 filaments; only 1-2 small unsynapsed stretches) and 'middle' (all other partially synapsed nuclei, most with 3-4 completed filaments). Nuclei in the 'late' category outnumbered the others in both *EmGFP-SYP-3; syp-3* and wild-type (N2) animals. This is consistent with the idea that each homolog pair initiates synapsis through an independent, stochastic process. Our observations agreed well with simulations based on independent initiation for each chromosome pair, using our measured rates of initiation and elongation.

Supplemental Movie Legends

Movie 1, related to Figure 1: Meiotic arrest upon immobilization
Nuclei from an *EmGFP-SYP-3; syp-3* hermaphrodite in which active chromosome motions cease after ~15min. 3D images were acquired at 1-minute intervals. Playback speed is 300x real-time. Elapsed time is indicated at lower right corner.

Movie 2, related to Figure 1: Meiotic arrest is bypassed by addition of serotonin
Time-lapse movie of transition zone nuclei from an *EmGFP-SYP-3; syp-3* hermaphrodite. Chromosome motion persists after 1:30 hours of imaging. 3D images were acquired every 1min. Playback speed is 300x real-time. Elapsed time is indicated at lower right corner.

Movie 3, related to Figure 1: EmGFP-SYP-3 is an SC marker for live imaging
3D rendering of the transition zone region in a live *EmGFP-SYP-3; syp-3* hermaphrodite.

Movie 4, related to Figure 2: Time-lapse imaging of SC assembly
A single nucleus from a time-lapse recording of an *EmGFP-SYP-3; syp-3* hermaphrodite shown in Figure 2A. 3D image stacks were acquired every 1min. Playback speed is 300x real-time. Elapsed time is indicated below the scale bar (lower left corner).

Movie 5, related to Figure 2: Time-lapse imaging of SC assembly
Time-lapse movie of a nucleus from an *EmGFP-SYP-3; syp-3* hermaphrodite also shown in Figure 2B. Images were acquired every 20sec. Playback speed is 150x real-time. Elapsed time is indicated at lower right corner.

Movie 6, related to Figure 2: Time-lapse imaging of synapsis initiation at PC
Time-lapse movie of the nucleus from an *EmGFP-SYP-3; syp-3; SUN-1-mRuby* hermaphrodite shown in Figure 2C. EmGFP-SYP-3 is shown in white, and SUN-1-mRuby is shown in magenta. Images were acquired every 1min. Playback speed is 300x real-time.

Movie 7, related to Figure 2: Time-lapse imaging of synapsis initiation at PC
Time-lapse movie of the nucleus from an *EmGFP-SYP-3; syp-3; SUN-1-mRuby* hermaphrodite shown in Figure 2D. EmGFP-SYP-3 is shown in white, and SUN-1-mRuby is shown in magenta. Images were acquired every 1min. Playback speed is 300x real-time.

Movie 8, related to Figure 4: Time-lapse imaging of SC assembly in the *sun-1(jf18)* mutant

Time-lapse movie of the nucleus from an *EmGFP-SYP-3; syp-3; sun-1(jf18)* hermaphrodite shown in Figure 4A. Images were acquired every 1min. Playback speed is 300x real-time. Elapsed time is indicated below the scale bar (lower left corner).

Movie 9, related to Figure 4: Time-lapse imaging of SC assembly in the *htp-1(gk174)* mutant

Time-lapse movie of the nucleus from an *EmGFP-SYP-3; syp-3; htp-1(gk174)* hermaphrodite shown in Figure 4B. Images were acquired every 1min. Playback speed is 150x real-time. Elapsed time is indicated below the scale bar (lower left corner).

Movie 10, related to Figure 2: Animated model of SC assembly

Animated model (based on Movie 6). Artist's rendering of the nuclear envelope (magenta circle), imaginary chromosome axes (green lines) and the SC (red bars) are superimposed on partial projections of a nucleus from an *EmGFP-SYP-3; syp-3; SUN-1-mRuby* hermaphrodite. EmGFP-SYP-3 is shown in white, and SUN-1-mRuby is shown in magenta. Images were acquired every 1min. Playback speed is 180x real-time.

Supplemental Experimental Procedures

Worm strains and transgenes

All strains were cultured using standard methods (Brenner, 1974). The following mutations and rearrangements were used:
syp-3(ok758) I; unc-119(ed3) III; htp-1(gk174) IV; sun-1(jf18) V; nT1[unc-?(n754) let-?] (IV;V); hT2[let-?(q782) qIs48] (I;III).

A transgene encoding EmGFP-SYP-3 (*ieSi11*) was constructed using the MosSCI repair template vector pCFJ150 (Frokjaer-Jensen et al., 2008). The genomic region encoding *syp-3*, including 395 bp upstream and 187 bp downstream of the coding sequence, was inserted into the multiple cloning site of pCFJ150. A synthetic gene encoding EmGFP followed by a 5xGly linker with *C. elegans* codon optimization (see *EmGFP* sequence below; (Tsien, 1998)), was inserted immediately upstream of the *syp-3* start codon by isothermal assembly (Gibson et al., 2009). This construct was integrated at the *ttTi5605 II* site by MosSCI (Frokjaer-Jensen et al., 2012; Frokjaer-Jensen et al., 2008), and later homozygosed. A single-copy insertion of the expected size was verified by PCR and Southern blot analysis (data not shown).

EmGFP-SYP-3 recapitulated the localization of SYP-3: it was first detected during early meiotic prophase as small nuclear aggregates and diffuse nucleoplasmic staining, gradually accumulated in linear segments at the interface between homologous chromosomes, and persisted along chromosomes until SC disassembly at diplotene-diakinesis (Figure 1A-B, Figure S3A, Movie 3 and (Smolikov et al., 2007)). EmGFP-SYP-3 expression did not confer any meiotic defects, as determined by cytological assessment of meiotic prophase and quantitative determination of embryonic viability and male self-progeny, sensitive readouts of meiotic nondisjunction in *C. elegans* (Figure S2A-C). Eliminating endogenous SYP-3 by crossing the transgenic animals to *syp-3(ok758)* null mutants enhanced the fluorescence associated with the SC, which enabled imaging over longer periods before excessive photobleaching.

The *EmGFP-SYP-3* reporter was validated in several ways: (1) hermaphrodites carrying only the fusion protein – i.e., lacking wild-type *syp-3* – produced broods of normal size, although frequencies of inviable and male progeny were slightly elevated relative to wild-type animals (Figure S2A-C). This indicates that most chromosomes segregate properly, which requires SC function (MacQueen et al., 2002). (2) No increase in the length of the transition zone was observed in *EmGFP-SYP-3; syp-3* relative to *EmGFP-SYP-3* hermaphrodites, indicating that pairing and synapsis were not significantly delayed (Figure S2D). (3) Based on high-resolution analysis of fixed tissue, the progression of synapsis in *EmGFP-SYP-3; syp-3* was indistinguishable from wild-type hermaphrodites

(Figure S4C). (4) Using images acquired at lower temporal resolution and assuming that SC filaments extend at constant rates, we estimated the median SC elongation rate to be 183nm/min and 180nm/min in *EmGFP-SYP-3; syp-3* and *EmGFP-SYP-3* worms, respectively (mean=195.7, 195.8; SD=49.4, 54.8; range 113-280, 100-300; Figure 3B-C), indicating that the absence of untagged SYP-3 does not markedly affect the kinetics of SC elongation.

SUN-1-mRuby (ie*Si21*) was created by cloning the *sun-1* coding sequence, together with 468 and 780 bp upstream and downstream, respectively. Codon-optimized mRuby (including a single intron from the *zyg-12* gene), together with a 3x(Gly-Gly-Ser-Gly) linker, was fused to the SUN-1 C-terminus, which resides in the perinuclear space between the inner and outer nuclear membranes (see *mRuby* sequence below; (Kredel et al., 2009; Tzur et al., 2006)). Cloning was done by isothermal assembly (Gibson et al., 2009). SUN-1-mRuby was integrated at the *cxTi10882 IV* site by MosSCI (Frokjaer-Jensen et al., 2012; Frokjaer-Jensen et al., 2008) and later homozygosed.

Expression of SUN-1-mRuby caused no discernible meiotic defects (Figure S2A-C). Its localization was indistinguishable from that of endogenous SUN-1: it localized to the nuclear envelope in embryonic and germline nuclei, and formed distinct 'patches' that colocalized with PCs in transition zone nuclei (Figure 1C and Figure S3B; (Penkner et al., 2007; Penkner et al., 2009; Sato et al., 2009)). These patches fused and split, and exhibited saltatory movements lasting a few seconds (Baudrimont et al., 2010; Wynne et al., 2012) – too transient to be detected under the imaging regime used here to track SC formation (usually one 3D image/min).

DNA sequence of codon-optimized EmGFP (the start codon is underlined):
ATGGTTTCTAAAGGAGAAGAACTTTTCACAGGAGTTGTTCCAATACTTGTTGAACTTGA
TGGAGATGTAAATGGACATAAGTTCTCTGTTTCTGGCGAAGGAGAAGGAGATGCTACT
TATGGAAAACTTACTCTCAAGTTCATTTGCACTACTGGAAAACTTCCCGTTCCATGGCC
AACTCTTGTTACTACTTTGACTTATGGAGTTCAATGTTTCGCTCGTTATCCAGACCATAT
GAAACAACACGATTTCTTCAAATCTGCTATGCCAGAAGGATATGTTCAAGAAAGAACTA
TTTTCTTCAAAGATGATGGAAACTACAAAACTCGTGCGGAAGTAAAGTTTGAGGGAGA
TACTCTTGTAAATAGAATAGAACTCAAAGGAATAGATTTCAAAGAAGATGGAAATATAC
TTGGACATAAACTTGAATATAACTACAATAGTCATAAAGTTTATATTACTGCTGATAAAC
AAAAAAATGGAATAAAAGTAAACTTCAAAACTCGTCATAATATAGAAGATGGAAGTGTT
CAACTTGCTGACCATTACCAACAAAATACTCCAATAGGAGATGGCCCAGTTCTTCTCCC
AGATAATCATTATCTTTCTACTCAATCTGCTCTTTCTAAAGACCCAAATGAAAAAAGAGA
CCATATGGTTCTTTTAGAGTTCGTTACTGCGGCGGGAATAACTCTTGGAATGGATGAA
CTTTACAAA

DNA sequence of codon-optimized mRuby (the start codon is underlined; the sequence in lower case is an intron from the *zyg-12* gene):

ATGAACTCTCTTATCAAGGAAAACATGCGCATGAAGGTTGTTCTTGAGGGATCTGTTAA
CGGACATCAGTTCAAGTGCACTGGAGAAGGAGAAGGAAATCCATACATGgtatgtgatacat
ggaaataggcacattcattaaatatttgtattttcagGGAACTCAAACTATGCGCATCAAGGTTATCGAAGG
AGGACCACTTCCATTCGCTTTCGACATCCTTGCTACCTCTTTCATGTACGGATCTCGCAC
TTTCATTAAGTATCCAAAGGGAATTCCAGATTTCTTCAAGCAGTCTTTCCCAGAAGGATT
CACTTGGGAGCGCGTTACCCGCTACGAGGATGGAGGAGTTATCACCGTTATGCAAGA
TACCTCCCTTGAGGATGGATGCCTTGTTTACCACGCTCAAGTTCGTGGAGTTAACTTCC
CATCTAACGGAGCTGTTATGCAGAAGAAGACTAAGGGATGGGAACCAAACACTGAAA
TGATGTACCCAGCTGATGGAGGACTTCGCGGATACACCCACATGGCTCTTAAGGTTGA
TGGAGGAGGACACCTTTCTTGCTCTTTCGTTACCACCTACCGCTCTAAGAAGACTGTTG
GAAATATTAAGATGCCAGGAATCCATGCTGTCGATCACCGTCTTGAGCGTCTTGAGGA
GTCTGATAACGAGATGTTCGTTGTTCAACGTGAGCACGCTGTCGCTAAGTTCGCTGGA
CTTGGAGGAGGA

Live imaging and image analysis

Adult hermaphrodites were immobilized on freshly prepared agarose pads (7.5% in water) overlayed with 100nm polystyrene beads (Polysciences, cat#00876; (Kim et al., 2013)). Except when otherwise noted, the pad and beads included freshly dissolved serotonin creatinine sulfate (Sigma) at a final concentration of 25mM. Addition of serotonin caused some bead aggregation, which is unlikely to directly impact meiotic progression (OR & AFD, unpublished observations). Worms were overlaid with high-performance coverslips (0.17 ± 0.005 mm; Schott) that were sealed to the slide with VALAP (1:1:1 vaseline:lanolin:parafin), and imaged immediately afterwards. 42.8% of worms maintained meiotic chromosome motions after 1 hour (n=320), with high slide-to-slide variability (10% to 90% per slide). In animals in which chromosome motion persisted, the rates of chromosome motion and synapsis did not change perceptibly over this time (Figure 3A and data not shown). The persistence of meiotic chromosome motions in individual wild-type animals immobilized in the presence of serotonin correlated with pharyngeal pumping (Fisher's exact test: $p<10^{-6}$; Figure S1C), indicating that the meiotic arrest reflects a holistic physiological response rather than a specific effect on the germline. We generally recorded images from the posterior gonad arm, the motion of which was less perturbed by pharyngeal pumping than the anterior arm. Only gonads for which chromosome motion was detected during the entire recording were analyzed, except where otherwise indicated.

Images were acquired using a Marianas spinning-disc confocal microscope (Intelligent Imaging Innovations, Inc. [3i]) at ambient temperature (19°C-24°C), using a 63x 1.4NA oil objective and 1.5x Optivar, yielding a pixel spacing of 113x113nm. 3D image stacks of 11-17 sections at 0.5µm z-spacing were acquired over 1-3 seconds, every 20-90 seconds. Typical settings were: 25ms exposure at 35% power for a 488nm laser to image EmGFP-SYP-3, and 15ms exposure at 75% power for a 561nm laser to image SUN-1-mRuby. These settings were optimized to minimize photobleaching over the course of our imaging, while allowing the discernment of subnuclear features.

Raw image stacks were analyzed using Imaris 7.3 (Bitplane). Time-lapse series were segmented, tracked and aligned based on overall fluorescence of EmGFP-SYP-3 using the Spots or Surface tools, and were validated by inspection. Filaments in informative nuclei were traced by hand from 3D reconstructions using the Measurement Point tool. 2-6 points were placed at the filament's termini and along its length at ~1µm intervals, and their 3D positions were confirmed by tilting of the reconstruction (Figure S1D). For analysis of synapsis initiation site we analyzed time-lapsed images with clear image of the first nascent 'filament' (0.5-1.0µm in length). In all cases analyzed (n=28) the filament at that early timepoint was abutted by a SUN-1 focus.

As with most observations of fluorescence in live specimens, the spatial and temporal resolution of these data were limited by photobleaching. The primary limitations were the axial resolution of confocal microscopy (~1µm under our conditions), noise, and temporal resolution (20-60secs), which were dictated by our efforts to limit phototoxicity and photobleaching during long-term imaging. A further limitation is imposed by the fact that synapsis takes place in the context of dynein-driven chromosome motions, which occur with dynamics that exceed those of SC assembly by two orders of magnitude (speed: 1.14×10^4 *versus* 1.6×10^2 nm/min; duration: 1.9 *versus* 1.5×10^3 sec; (Wynne et al., 2012)). These limitations impose a measure of uncertainty on any single measurement, and likely account for the majority of the fluctuations in our plots (e.g., Figure 3A). Our reliance on linear regression to measure synapsis rates, rather than on specific timepoints, partially mitigates this issue. Both uncertainties in our measurements and limited temporal resolution prevent us from ruling out a discontinuous elongation process in which pauses are shorter than a few timepoints (i.e., 4-5mins).

Data analysis and simulations

SC length plots were subjected to segmented linear regression, minimizing the residuals with a maximum of one breakpoint to designate the elongating and constant-length

segments. The best-fitted elongating portions of the plots are shown as red lines in the SC length plots throughout the figures.

Simulations were performed by considering the synapsis state of 6 homolog pairs. Each pair was assigned an equal chance of initiating synapsis per minute. Following initiation, filaments elongated at a constant rate, until they were defined as 'visible' (>0.85μm), or 'complete' (>3.5μm). At least 1000 independent simulations were performed for each condition. Data analysis and simulations were performed in Matlab 7.14 (MathWorks), using custom code (available upon request).

Immunofluorescence and analysis of immobilized worms

Immunofluorescence was performed as previously described (Phillips et al., 2009). The following antibodies were used: anti-SYP-2 (rabbit, affinity purified, 1:1,000), anti-GFP (mouse monoclonal, Abcam, 1:200), anti-SUN-1 (rabbit, affinity-purified, SDI, 1:10,000), anti-HTP-3 (guinea pig, 1:500), anti-HIM-8 (rat, 1:500) and appropriate secondary antibodies conjugated to dyes (1:500). Imaging was performed using Marianas spinning-disc confocal microscope (Intelligent Imaging Innovations, Inc. [3i]) with a 63x 1.4NA oil objective or a 100x 1.46NA oil objective, and 1.5x Optivar. 3D stacks were visualized in Imaris 7.3 (Bitplane).

Transition zone length was ascertained based on imaging of intact immobilized worms expressing EmGFP-SYP-3 and SUN-1-mRuby. The transition zone was defined as the region of the gonad where majority of nuclei have multiple SUN-1 foci.

Supplemental References

Baudrimont, A., Penkner, A., Woglar, A., Machacek, T., Wegrostek, C., Gloggnitzer, J., Fridkin, A., Klein, F., Gruenbaum, Y., Pasierbek, P., *et al.* (2010). Leptotene/zygotene chromosome movement via the SUN/KASH protein bridge in Caenorhabditis elegans. PLoS Genet *6*, e1001219.

Brenner, S. (1974). The genetics of Caenorhabditis elegans. Genetics *77*, 71-94.

Frokjaer-Jensen, C., Davis, M.W., Ailion, M., and Jorgensen, E.M. (2012). Improved Mos1-mediated transgenesis in C. elegans. Nat Methods *9*, 117-118.

Frokjaer-Jensen, C., Davis, M.W., Hopkins, C.E., Newman, B.J., Thummel, J.M., Olesen, S.P., Grunnet, M., and Jorgensen, E.M. (2008). Single-copy insertion of transgenes in Caenorhabditis elegans. Nat Genet *40*, 1375-1383.

Gibson, D.G., Young, L., Chuang, R.Y., Venter, J.C., Hutchison, C.A., 3rd, and Smith, H.O. (2009). Enzymatic assembly of DNA molecules up to several hundred kilobases. Nat Methods *6*, 343-345.

Kim, E., Sun, L., Gabel, C.V., and Fang-Yen, C. (2013). Long-term imaging of Caenorhabditis elegans using nanoparticle-mediated immobilization. PLoS One *8*, e53419.

Kredel, S., Oswald, F., Nienhaus, K., Deuschle, K., Rocker, C., Wolff, M., Heilker, R., Nienhaus, G.U., and Wiedenmann, J. (2009). mRuby, a bright monomeric red fluorescent protein for labeling of subcellular structures. PLoS One *4*, e4391.

MacQueen, A.J., Colaiacovo, M.P., McDonald, K., and Villeneuve, A.M. (2002). Synapsis-dependent and -independent mechanisms stabilize homolog pairing during meiotic prophase in C. elegans. Genes Dev *16*, 2428-2442.

Penkner, A., Tang, L., Novatchkova, M., Ladurner, M., Fridkin, A., Gruenbaum, Y., Schweizer, D., Loidl, J., and Jantsch, V. (2007). The nuclear envelope protein Matefin/SUN-1 is required for homologous pairing in C. elegans meiosis. Dev Cell *12*, 873-885.

Penkner, A.M., Fridkin, A., Gloggnitzer, J., Baudrimont, A., Machacek, T., Woglar, A., Csaszar, E., Pasierbek, P., Ammerer, G., Gruenbaum, Y., *et al.* (2009). Meiotic chromosome homology search involves modifications of the nuclear envelope protein Matefin/SUN-1. Cell *139*, 920-933.

Phillips, C.M., McDonald, K.L., and Dernburg, A.F. (2009). Cytological analysis of meiosis in Caenorhabditis elegans. Methods Mol Biol *558*, 171-195.

Sato, A., Isaac, B., Phillips, C.M., Rillo, R., Carlton, P.M., Wynne, D.J., Kasad, R.A., and Dernburg, A.F. (2009). Cytoskeletal forces span the nuclear envelope to coordinate meiotic chromosome pairing and synapsis. Cell *139*, 907-919.

Smolikov, S., Eizinger, A., Schild-Prufert, K., Hurlburt, A., McDonald, K., Engebrecht, J., Villeneuve, A.M., and Colaiacovo, M.P. (2007). SYP-3 restricts synaptonemal complex assembly to bridge paired chromosome axes during meiosis in Caenorhabditis elegans. Genetics *176*, 2015-2025.

Tsien, R.Y. (1998). The green fluorescent protein. Annu Rev Biochem *67*, 509-544.

Tzur, Y.B., Wilson, K.L., and Gruenbaum, Y. (2006). SUN-domain proteins: 'Velcro' that links the nucleoskeleton to the cytoskeleton. Nat Rev Mol Cell Biol *7*, 782-788.

Wynne, D.J., Rog, O., Carlton, P.M., and Dernburg, A.F. (2012). Dynein-dependent processive chromosome motions promote homologous pairing in C. elegans meiosis. J Cell Biol *196*, 47-64.